Violation of the rule of parsimony: Mixed local moment and itinerant Fe magnetism in Fe_3GeN

Mari Tsumuraya [1] and David J. Singh [1,2,3,*]

[1]*Department of Physics and Astronomy, University of Missouri, Columbia, Missouri 65211, USA*

[2]*Department of Chemistry, University of Missouri, Columbia, Missouri 65211, USA*

[3]*Department of Mechanical and Aerospace Engineering, University of Missouri, Columbia, Missouri 65211, USA*

(Received 27 April 2022; accepted 30 June 2022; published 12 July 2022)

Ternary iron nitrides are of considerable interest due to their diverse magnetic properties. We find, based on first principles calculations, that the relatively minor structural distortion from the cubic antiperovskite structure in Fe_3GeN, consisting of octahedral rotations, leads to unusual magnetic behavior. In particular, there is a separation into Fe sites with very different magnetic behaviors, specifically a site with Fe atoms having a stable local moment and a site where the Fe shows characteristics of much more itinerant behavior. This shows a remarkable flexibility of the Fe magnetic behavior in these nitrides and points towards the possibility of systems where minor structural and chemical changes can lead to dramatic changes in magnetic properties. The results suggest that, analogously to oxide perovskite materials, modulation of magnetic properties via chemical or strain control of octahedral rotation may be feasible. This may then lead to approaches for tuning magnetism to realize properties of interest, for example, tuning magnetic transitions to quantum critical regimes or to proximity to metamagnetic transitions of interest for devices.

DOI: 10.1103/PhysRevB.106.024408

I. INTRODUCTION

Iron nitride compounds and particularly their magnetic properties have been the subject of considerable interest. This was stimulated by reports of exceptional magnetic properties in tetragonal $Fe_{16}N_2$, including high magnetization in combination with reasonable coercivity for many applications [1–3]. Related to this, Fe shows a remarkable variety of magnetic behaviors depending on structure. For example, the ground-state bcc structure of α-Fe is a well-known ferromagnet, while austenite, a fcc structure, shows much weaker magnetism and lies higher in energy because of this difference [4,5]. Other binary Fe-N compounds include Fe_3N, which is hexagonal and ferromagnetic [6], and Fe_4N, which is cubic, with a lattice consisting of Fe on fcc sites and N in octahedral holes. This compound, despite its fcc Fe sublattice, has a substantial magnetization of $2.14\mu_B$/Fe, similar to bcc Fe [7,8].

Ternary iron-nitride compounds provide opportunities for better understanding the relationships between structure and magnetism in iron-rich phases, but have been relatively less investigated as compared with the binary phases. Some examples include $GaFe_3N$, which is an antiferromagnet [9], and Fe_3RhN, which is an itinerant ferromagnet with a magnetic moment of $8.3\mu_B$ per formula unit [10]. These compounds form in the cubic antiperovskite structure, which is the same as the structure of Fe_4N, with one Fe substituted by another element. The antiperovskite structure may thus be regarded as fcc Fe with one quarter of the Fe atoms substituted by another element to yield a simple cubic lattice and N inserted into Fe coordinated octahedral holes. Here we show that there can be a large sensitivity to structural distortions similar to perovskite oxides, and in particular that for Fe_3GeN octahedral rotation leads to two very distinct Fe sites from the point of view of their magnetic behavior. This contradicts the expectation from the rule of parsimony, which is the principle that a given element generally has a minimum number of physically distinct sites or behaviors in a stable compound.

Other Fe-N ternary phases with this antiperovskite structure include $AlFe_3N$ [11] and ferromagnetic $ZnFe_3N$ [11,12]. Antiperovskite intermetallics, stoichiometry AFe_3N, where A is a metal or metalloid, normally form in the undistorted cubic ABO_3 perovskite type structure, space group $Pm\bar{3}m$ with A on the perovskite A site (0,0,0), Fe on the perovskite O site $(0, \frac{1}{2}, \frac{1}{2})$, $(\frac{1}{2}, 0, \frac{1}{2})$, $(\frac{1}{2}, \frac{1}{2}, 0)$, and N on the perovskite B site $(\frac{1}{2}, \frac{1}{2}, \frac{1}{2})$. The perovskite structure is often described as consisting of corner-sharing BO_6 octahedra and A-site cations in the large interstices between these octahedra. Oxide perovskites most commonly distort from the cubic structure by rotations and tilts of the BO_6 octahedra [13]. Antiperovskite intermetallics are distinct in this regard in that they normally form in the ideal cubic structure, without distortions.

Iron germanium nitride Fe_3GeN is exceptional in this regard. In particular, it has an antiperovskite based tetragonal structure, which consists of corner-sharing NFe_6 octahedra that are alternately rotated along the c axis of a tetragonal cell, similar to many oxide perovskites (see Fig. 1). Interestingly, while not common among intermetallic antiperovskite compounds, octahedral rotation and tilts are very important in modifying the properties of oxide perovskites [14–16]. Scholz and Dronskowski [17] found that the structure of $Fe_{4-x}Ge_xN_y$ changes from a cubic antiperovskite structure to the distorted tetragonal structure with increasing content of Ge replacing Fe. Liu and coworkers showed that this transition is

*singhdj@missouri.edu

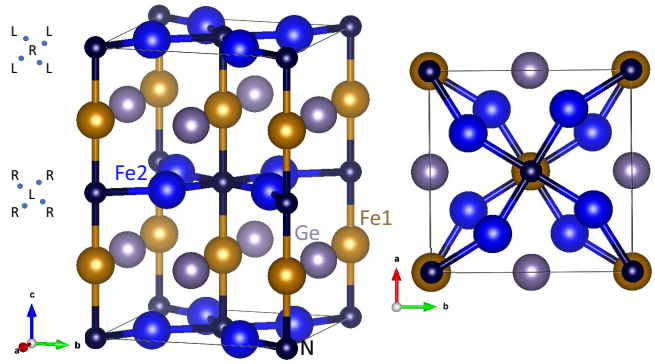

FIG. 1. Crystal structure of Fe_3GeN shown in two views as indicated. The atomic positions are as optimized by energy minimization using the PBE GGA. Note the alternating rotation of the NFe_6 octahedra around the c axis, as indicated by the schematics for two layers on the left side of the figure.

continuous as a function of Ge content in $Fe_{4-x}Ge_xN$ [18]. In any case, Fe_3GeN, which shows a net magnetic moment $0.2\mu_B$–$0.3\mu_B$ per Fe with sample dependence, has tetragonal symmetry at room temperature [17,19]. This structure has a doubled primitive unit cell containing two formula units, space group $I4/mcm$, number 140.

Previous studies report some unusual physical behavior, including an unusual critical behavior. This is reported to be intermediate between the expected short-range Heisenberg-type behavior and more long-range behavior [20]. In addition, an anomalous Hall effect is reported [21]. One complication has been that the compound may form off stoichiometry, in particular with partial filling of the N sites [17,19]. This tendency to variable stoichiometry complicates analysis of the physical properties. Reported experimental lattice parameters are $a = 5.231$ Å, $c = 7.658$ Å for $GeN_{0.5}Fe_3$ [19], and $a = 5.3053$ Å, $c = 7.7632$ Å for Fe_3GeN [20]. The difference between them is presumably mainly due to the nitrogen stoichiometry.

In any case, octahedral rotations lead to distinct Fe sites, specifically the three Fe atoms in the formula unit are divided into two-plane Fe atoms and an apical Fe atom, which may then behave differently with respect to formation of the electronic structure. These are the Fe1 site (Wycoff site, 4*a*, one atom per formula unit, two per primitive cell) and the Fe2 site (Wycoff site 8*h*, two atoms per formula unit, four per primitive cell). Considering the intersecting chains of Fe and N atoms along the Cartesian directions that are characteristic of the perovskite structure, the octahedral rotation in Fe_3GeN leaves straight ...Fe1-N-Fe1-N... chains along the c-axis direction, while the ...Fe2-N-Fe2-N... chains in the in-plane directions become bent, specifically with N-Fe-N bond angles that deviate from 180°. The calculated octahedral rotation angle for the PBE GGA at the experimental lattice parameters is 13.24°, leading to a N-Fe2-N bond angle of 153.52°. Prior theoretical work has shown that the ferromagnetic moment observed is a consequence of a ferrimagnetic ordering of the Fe1 and Fe2 itinerant moments associated with Fe d states around the Fermi level [18]. The presence of Fe d dominated electronic states near the Fermi level and associated magnetism is a common feature of Fe-based antiperovskite nitrides [22,23]. The purpose of the present work is to investigate the effects of the structural separation into two distinct Fe sites.

II. COMPUTATIONAL METHODS

The present first principles work was done within density-functional theory using general potential linearized augmented plane-wave (LAPW) method [24], as implemented in the WIEN2K code [25]. The reported results were obtained using LAPW sphere radii of 2.30 Bohr, 1.55 Bohr, and 2.00 Bohr for Ge, N, and Fe, respectively. We tested other choices of sphere radii and used somewhat smaller sphere radii of 1.85 Bohr for Fe in the determination of the equilibrium lattice parameters in order to avoid sphere overlaps. The calculations were done with well-converged, tested choices for the basis set cutoff and the Brillouin zone sampling. The results shown were obtained with Brillouin-zone sampling by $16 \times 16 \times 16$ uniform **k**-point meshes. We did calculations with both the common Perdew, Burke, and Ernzerhof generalized gradient approximation (PBE GGA) [26] and with the local density approximation (LDA) due to the possible sensitivity of results on magnetism of a Fe-based intermetallic to the particular functional [5]. The differences may be regarded as an indication of uncertainty due to the choice of the functional.

The nature of the magnetism was studied using constrained density-functional theory (DFT) [27]. This allows calculations of the energy and other properties, for example, contributions of different sites to the magnetism, as a function of a constraint. Here we used the fixed spin moment method [28,29], where the constraint is on the total spin magnetization of the unit cell. This constraint is imposed by fixing the difference between the spin-up and spin-down occupations. This leads to a difference in Fermi energy between spin-up and spin-down corresponding to the constraining field [24].

We did calculations at the reported experimental lattice parameters of $a = 5.3053$ Å, and $c = 7.7632$ Å [20], and also as a function of lattice parameters. In all cases, we relaxed the free internal coordinates, specifically the in-plane Fe2 position, which is related to the octahedral rotation. For the PBE functional at the experimental lattice parameters, we obtained a Fe2 position of (0.691,0.191,0). This corresponds to a larger rotation than that for the coordinate reported by Boller and coworkers [19], who obtained (0.73,0.23,0) for samples with a reported stoichiometry $Fe_3GeN_{0.51}$. The lower rotation in that report is intermediate between the unrotated cubic structure of Fe_3Ge and our result for stoichiometric Fe_3GeN. Interestingly, this trend is also consistent with the trends for oxide ABO_3 perovskite materials. In those oxides, increasing the B-site size (N here), while keeping the A site fixed, reduces the perovskite tolerance factor $t = (r_A + r_O)/\sqrt{2}(r_B + r_O)$, where r_A, r_B, and r_O are the ionic radii of A, B, and O, respectively [30].

Reduction of the tolerance factor in normal perovskites generally leads to stronger octahedral rotation. One may also rationalize the result of Scholz and Dronskowski in this picture. They reported that $Fe_{4-x}Ge_xN_y$ changes from cubic to tetragonal as x increases [17]. This is by noting that Ge is smaller than Fe, based on trends in transition-metal germanides, also consistent with a shrinking unit cell volume as Fe is alloyed with Ge. Thus the tolerance factor is decreased

TABLE I. Ground states from self-consistent field calculations. M_{total} is the total magnetic moment per six Fe atom unit cell. M_{Fe1} and M_{Fe2} are the Fe1 and Fe2 magnetic moments from integration of the spin densities in the LAPW spheres, and are given per atom. Note that spin density also has small components outside the Fe spheres, which accounts for the difference between the total moment per cell and the sum of the Fe moments. These are given at the experimental and at the calculated lattice parameters a and c for the LDA and PBE functionals. Note that the unit cell contains two Fe1 atoms and four Fe2 atoms.

Functional	Experimental lattice parameters				Theoretical lattice parameters			
	Lattice parameters (Å)	Magnetic moment (μ_B)			Lattice parameters (Å)	Magnetic moment (μ_B)		
		M_{total}	M_{Fe1}	M_{Fe2}		M_{total}	M_{Fe1}	M_{Fe2}
PBE	$a = 5.3053$ $c = 7.7632$	4.66	1.86	0.31	$a = 5.2133$ $c = 7.7638$	4.47	1.72	0.30
LDA	$a = 5.3053$ $c = 7.7632$	4.24	1.66	0.29	$a = 5.1072$ $c = 7.5312$	3.23	1.07	0.30

and the tendency to rotation is increased when the Fe on the A site is replaced by Ge. Thus while the bonding of these compounds is covalent and metallic [22], and not ionic as in the oxide perovskites, some of the structural rules, in particular the role of atomic sizes carry over.

III. RESULTS AND DISCUSSION

We begin with the ground-state properties. Lattice parameters and magnetic moments are summarized in Table I. The differences between the LDA and PBE results are typical of DFT calculations. The LDA gives somewhat lower magnetic moments and magnetization than the PBE, specifically a magnetization of $0.71\mu_B$ vs $0.78\mu_B$ per Fe at the experimental lattice parameter. It also predicts smaller lattice parameters than PBE, with an equilibrium cell volume that is 7% smaller. It may also be noted that the calculated c/a ratios (1.49 for PBE and 1.47 for LDA) are slightly larger than the experimental value of 1.46. In any case, the magnitude and direction of the differences in lattice parameters between the LDA and PBE functionals is typical of the behavior of these functionals in weakly and moderately correlated metals, including bulk Fe [31,32]. As mentioned, the experimental magnetization is sample dependent. However, it is generally somewhat smaller than our result. For example, a recent experimental study reported $0.57\mu_B$ per Fe for $Ge_{0.97}Fe_{3.03}N_{0.56}$ [17]. This may be a consequence of differences in stoichiometry or DFT errors. Interestingly, the type of deviation, where the experimental magnetization is smaller than the calculated LDA magnetization, is characteristic of some itinerant magnetic systems that are near quantum critical points. In particular, standard density-functional calculations, as with the LDA or PBE GGA, do not include renormalization of the magnetization due to spin-fluctuations near the critical point [33–35]. It may be of interest to experimentally study Fe_3GeN in this context as well as to perform detailed experimental studies of the connection between magnetic behavior and nitrogen stoichiometry.

Turning to the details of the ground-state magnetic behavior, one notes that the two inequivalent Fe sites behave very differently. The magnetization is mainly from the Fe1, apical Fe, site, while the in-plane Fe2 site has a much smaller moment. As mentioned, the Fe2 site differs from the Fe1 site in that it has bent N-Fe-N bonds due to the rotation. The magnetic moment of each Fe1 atom almost six times larger than that of a Fe2 atom. In our calculations, while the Fe2 moment is small, it is aligned ferromagnetically with the Fe1 moment.

Figure 2 shows the band structures for majority and minority spin. These are for the PBE functional at the experimental lattice parameters. The corresponding density of states (DOS) is given in Fig. 3. Our calculated DOS is in accord with the prior calculation of Liu and coworkers [18]. The Fermi level falls in a dip in the DOS. Fe d states dominate the DOS between -4 and 2 eV relative to the Fermi level. There is considerable hybridization evident in the DOS as seen also in prior work [18], and the projected band structure presented in the Appendix. As mentioned, the magnetic behaviors of the Fe1 and Fe2 sites are different. The analysis is somewhat complicated by the hybridization of the Fe1 and Fe2 states. Nonetheless, the Fe1 and Fe2 projections of the DOS are significantly different from each other. In particular, the Fe2 d DOS, besides showing smaller exchange splitting,

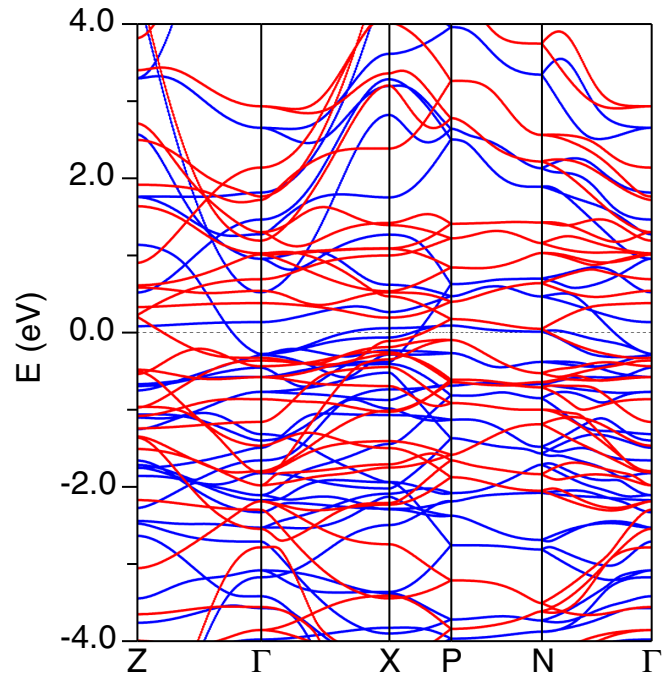

FIG. 2. Calculated band structure for majority and minority spin. The dashed line denotes the Fermi level at 0 eV. Majority-spin bands are shown in blue and minority-spin bands in red.

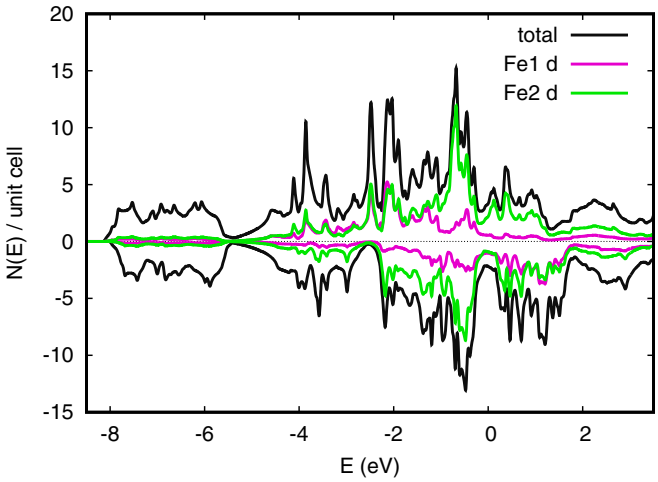

FIG. 3. Total and partial electronic density of states (DOS) plots shown on a per unit cell, two formula unit, basis. Majority- and minority-spin DOS are shown above and below zero, respectively. The Fermi level is at zero energy.

corresponding to the lower moment, appears more narrow, in particular for the peak that occurs just below the Fermi level. The density of states at the Fermi level, $N(E_F)$ are 3.32 and 2.19 eV^{-1} per six Fe atom unit cell, for majority and minority spins, respectively. Fat band plots for the region close to the Fermi energy, showing the Fe1 and Fe2 d characters, are given in the Appendix.

Several bands cross the Fermi level, as seen in the band structure. These lead to large Fermi surfaces in both the majority and minority spins. It is noteworthy that these bands are more dispersive in the k_z direction, i.e., Γ-Z, than in the in-plane direction. The Fermi surfaces are shown in Fig. 4. The majority spin shows hole-like rings around the zone edges and a small electron-like surface around the zone center, in addition to a large surface. The occupancies of the corresponding three partially filled majority-spin bands are 0.966, 0.319, and 0.045. The minority spin has one large sheet of Fermi surface, corresponding to a band with an occupancy of 0.670. The difference between the Fe1 and Fe2 sites is also reflected in the Fermi surface. In particular, it is significantly anisotropic between the k_z and the in-plane k_x and k_y directions, perpendicular to k_z. The large surfaces are flattened along k_z, particularly for the majority spin. This reflects the higher dispersion of the bands in this direction, leading to the expectation that the electrical conductivity should be higher in the c-axis direction, relative to in-plane.

We used constrained density-functional theory, fixed spin moment calculations to elucidate the nature of the magnetism [28,29]. These were done both at the experimental lattice parameter, and under uniform compression and expansion, for both the PBE and LDA functionals. We relaxed the internal coordinates of the Fe2 atom for each magnetization and volume. Figure 5 gives the results of fixed spin moment calculations for lattice parameters of 98%, 99%, 100%, and 101% of the experimental lattice values [20]. The energies and magnetization are shown on a per unit cell basis. The energy minimum for the experimental lattice parameters (curves marked 100% in comparison with the data in the first set

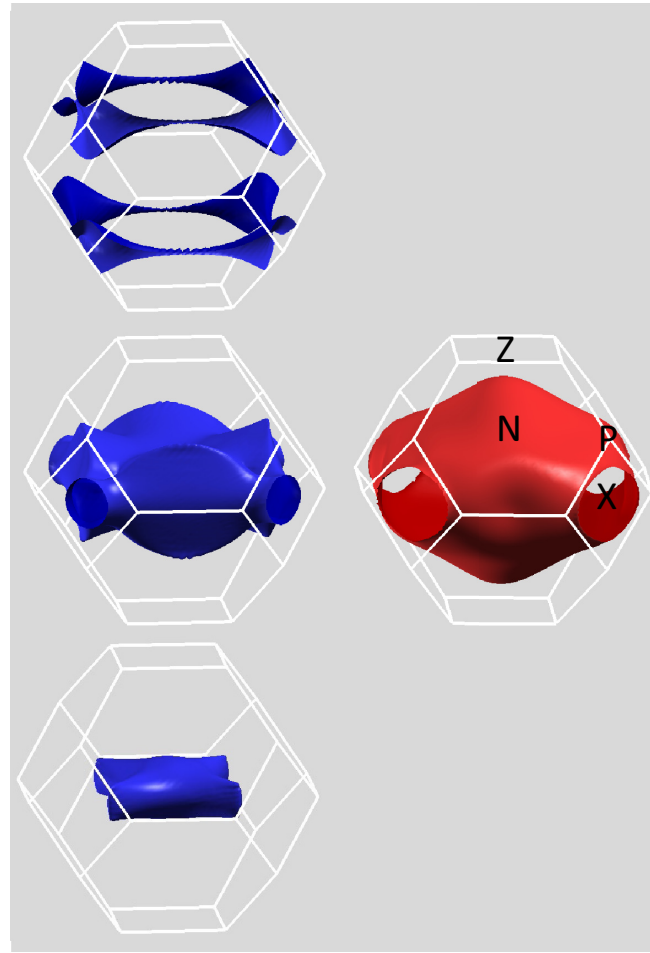

FIG. 4. Calculated Fermi surfaces for the PBE functional at the experimental lattice parameters. There are three majority-spin Fermi surfaces, shown in blue (left), and one minority-spin surface, shown in red (right). Γ is at the center of the body-centered tetragonal zone as shown. Other symmetry points corresponding to the points in the band structure are as indicated on the minority-spin surface (right). With respect to the conventional tetragonal zone, Z is along the k_z [0,0,1] direction, while X is along the conventional cell [1,1,0] direction.

of columns in the table) corresponds to the self-consistent magnetization shown in Table I, as expected. In addition, there is a flattening of the energy vs magnetization in the vicinity of $10\mu_B$ per unit cell ($\approx 1.7\mu_B$/Fe). This is with respect to the expected parabolic increase of the energy with magnetization and is particularly noticeable for the expanded cell and the PBE functional. This suggests proximity to a metamagnetic transition from the ground state to a high magnetization state, which might be found in high-magnetic-field experiments.

Figure 6 shows the magnetic moment of individual Fe1 and Fe2 atoms as a function of unit-cell magnetization in the fixed spin moment calculations. Although the Fe1 and Fe2 atoms are in chemically similar environments with similar coordination, they show dramatically different behaviors. The Fe2 moments are approximately linear with constrained magnetization for both functionals and for the different lattice parameters. The Fe1 moments on the other hand, while they do vary, are much less flexible. This is in the sense that,

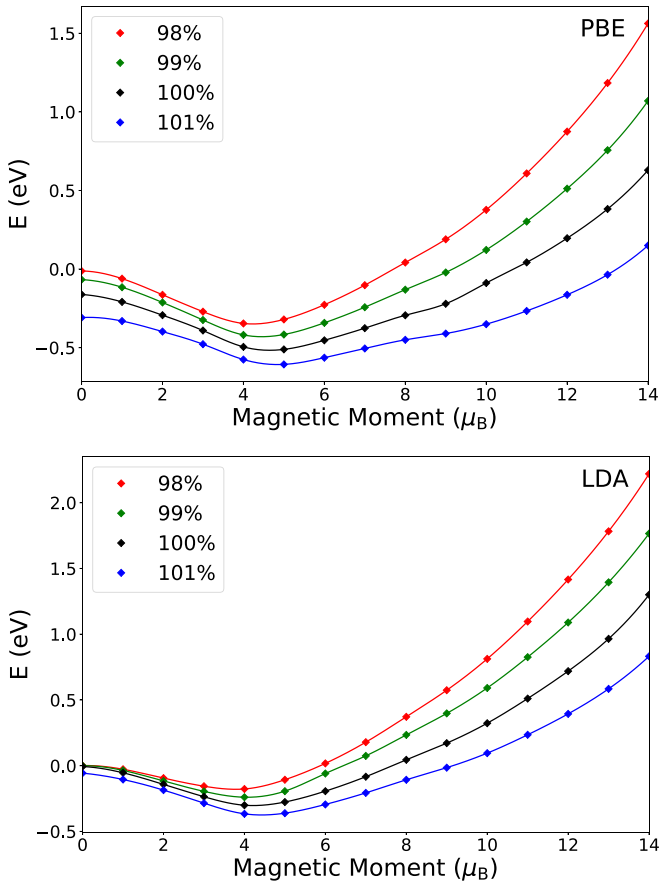

FIG. 5. Calculated fixed spin moment magnetic energy as a function of magnetization on a per unit cell basis, using the PBE and LDA functionals. The energy zero is taken as the energy of a non-spin-polarized calculation for each set of lattice parameters. The constrained zero moment per unit cell calculation can have a lower energy than the non-spin-polarized zero energy, as a consequence of forming a lower energy state with canceling nonzero moments on the Fe1 and Fe2 sites. This is seen at larger lattice parameters (99% and larger for PBE and 101% for LDA).

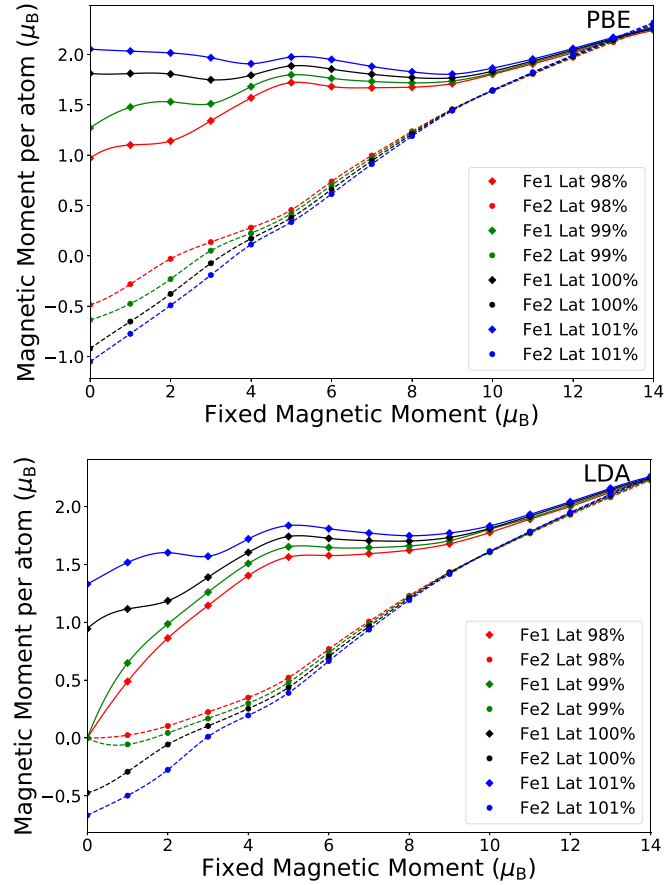

FIG. 6. Fe1 and Fe2 moment on a per atom basis versus constrained magnetization per unit cell from fixed spin moment calculations.

particularly for the PBE functional and for the experimental and expanded lattice parameter, the Fe1 moments do not show nearly as strong a dependence on magnetization as the Fe2 site. Thus when the total magnetization is constrained to have a value different from the equilibrium value the constraint is accommodated mainly by the Fe2 site.

Transition-metal magnets are often characterized according to the extent to which they show itinerant or local moment magnetism. The local moment limit has stable moments, and the magnetic behavior is governed by the interactions between the directions of these, as in the Heisenberg model, exemplified by many oxides, such as MnO.

The opposite itinerant limit is characterized by moments whose magnitude is variable and changes for example with temperature, such as, for example, in the Stoner picture, exemplified by fcc Ni. Based on the results in Fig. 6, the magnetic moment of Fe2 goes up strongly as the fixed spin moment increases in contrast to the behavior of the Fe1, which is relatively invariant. This means that the Fe1 atoms behave as if they have local moments, while the Fe2 atoms show a more itinerant nature. Thus, the magnetism of Fe_3GeN could be described as local Fe1 moments interacting through an itinerant system comprised by the Fe2 atoms. This result is robust. We find this differentiation of the Fe1 and Fe2 sites, both with the LDA and PBE functionals, at the experimental and the calculated lattice parameters and over a range of volumes around the experimental volume.

This nature could in principle be probed by neutron-diffraction measurements of the Fe1 and Fe2 moments as a function of temperature. While Fe_3GeN does not have a particularly high Curie temperature, it is notable that some very high Curie temperature materials, particularly Heusler Co_2FeSi ($T_c \simeq 1100$ K) show a similar characteristic [36]. In any case, the results show that in spite of their very similar chemical and coordination environments the magnetic behaviors of the two Fe sites in Fe_3GeN are very different. This reflects a sensitive interplay of structure and magnetism in a Fe compound.

IV. SUMMARY AND CONCLUSIONS

We report a DFT investigation of the ternary iron nitride compound, Fe_3GeN, which has a distorted antiperovskite structure, in which octahedral rotation leads to two distinct Fe sites. Remarkably, this also leads to very different magnetic properties of these Fe atoms. One site, the Fe1 apical site,

accounts for most of the magnetization and has a relatively stable moment. The other site Fe2, which is the in-plane Fe site, has a moment that is aligned with the Fe1 moment but is much smaller and much more flexible than the Fe1 moment. The magnetism may then be described as local Fe1 moments embedded in an itinerant Fe2 background. This separation into two sites with very different behavior is an unexpected deviation from the rule of parsimony, according to which the different Fe atoms would be expected to behave similarly.

The results suggest that, analogously to oxide perovskite materials, modulation of magnetic properties via chemical or strain control of octahedral rotation may be feasible. This may then lead to approaches for tuning magnetism to realize properties of interest, for example, tuning magnetic transitions to quantum critical regimes or to proximity to metamagnetic transitions of interest for devices. It will be of strong interest to extract rational design principles, analogous to those in oxides, for understanding and predicting the variation of structure with chemistry, order, strain and other parameters for these intermetallic antiperovskite phases.

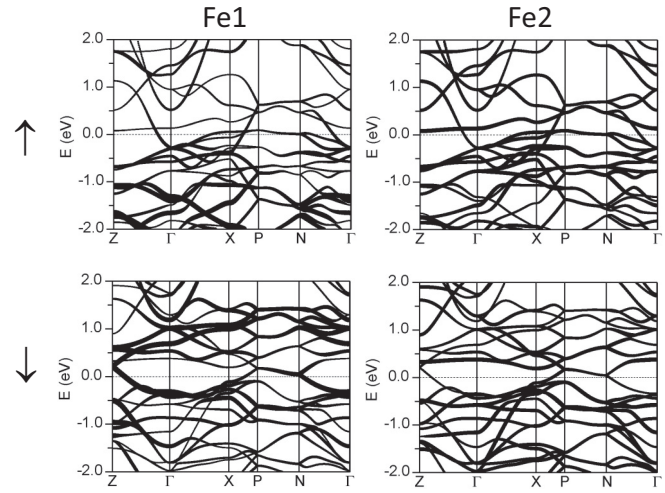

FIG. 7. Calculated projected band structures for majority spin (top) and minority spin (bottom). The dashed line denotes the Fermi level at 0 eV. The projections are on a per atom basis.

ACKNOWLEDGMENTS

We are grateful for helpful discussions with B.-H. Lei. This work was supported by the Department of Energy, Office of Basic Energy Science, Award No. DE-SC0019114.

APPENDIX

The projected band structures of Fe1d and Fe2d character for majority and minority spins near the Fermi energy E_F are shown in fat-band representations in Fig. 7. The projections were onto the corresponding LAPW spheres. As seen, the bands closest to E_F have hybridized Fe d character from the two sites.

Fe2 makes larger contributions for the majority spin, while Fe1 makes larger contributions for the minority spin in the energy range shown. This may also be noted from the density of states.

[1] K. H. Jack, Proc. R. Soc. London **195**, 34 (1948).
[2] M. Takahashi, H. Shoji, H. Takahashi, H. Nashi, and T. Wakiyama, J. Appl. Phys. **76**, 6642 (1994).
[3] J.-P. Wang, J. Magn. Magn. Mater. **497**, 165962 (2020).
[4] B. L. Bramfitt, in *Metals Handbook, Desk Edition, 2nd. Ed.*, edited by J. R. Davis (ASM International, Materials Park, 1998), p. 153.
[5] Y. Fu and D. J. Singh, Phys. Rev. Lett. **121**, 207201 (2018).
[6] A. M. Zieschang, J. D. Bocarsly, M. Durrshnabel, L. Monica-Luna, H. J. Kleebe, R. Seshadri, and B. Albert, Chem. Mater. **29**, 621 (2017).
[7] S. K. Chen, S. Jin, T. H. Tiefel, Y. F. Hsieh, E. M. Gyorgy, and D. W. Johnson, Jr., J. Appl. Phys. **70**, 6247 (1991).
[8] J. L. Costa-Kramer, D. M. Borsa, J. M. Garcia-Martin, M. S. Martin-Gonzalez, D. O. Boerma, and F. Briones, Phys. Rev. B **69**, 144402 (2004).
[9] J. Burghaus, M. Wessel, A. Houben, and R. Dronskowski, Inorg. Chem. (Washington, DC, US) **49**, 10148 (2010).
[10] A. Houben, P. Muller, J. Appen, H. Lueken, R. Dr, and R. Dronskowski, Angew. Chem., Int. Ed. **44**, 7212 (2005).
[11] Y. Fu, S. Lin, and B. Wang, J. Magn. Magn. Mater. **378**, 54 (2015).
[12] R. Niewa, Eur. J. Inorg. Chem. **2019**, 3647 (2019).
[13] A. M. Glazer, Acta Crystallogr., Sect. B: Struct. Crystallogr. Cryst. Chem. **28**, 3384 (1972).
[14] J. He, A. Borisevich, S. V. Kalinin, S. J. Pennycook, and S. T. Pantelides, Phys. Rev. Lett. **105**, 227203 (2010).
[15] J. M. Rondinelli and C. J. Fennie, Adv. Mater. **24**, 1961 (2012).
[16] D. I. Bilc and D. J. Singh, Phys. Rev. Lett. **96**, 147602 (2006).
[17] T. Scholz and R. Dronskowski, J. Mater. Chem. C **5**, 166 (2017).
[18] C. Liu, C. Zhang, X. Kan, X. Liu, S. Feng, Y. Yang, Q. Lv, J. Hu, and M. Shezad, J. Phys. Chem. C **124**, 6321 (2020).
[19] H. Boller, Monatsh. Chem. **99**, 2444 (1968).
[20] X. C. Kan, B. S. Wang, L. Zhang, L. Zu, S. Lin, J. C. Lin, P. Tong, W. H. Song, and Y. P. Sun, Phys. Chem. Chem. Phys. **19**, 13703 (2017).
[21] X. C. Kan, B. S. Wang, L. Zu, S. Lin, J. C. Lin, P. Tong, W. H. Song, and Y. P. Sun, RSC Adv. **6**, 104433 (2016).
[22] P. Mohn, K. Schwarz, S. Matar, and G. Demazeau, Phys. Rev. B **45**, 4000 (1992).
[23] A. V. G. Rebaza, J. Desimoni, S. Kurian, S. Bhattacharyya, N. S. Gajbhiye, and E. P. Y. Blancá, J. Phys. Chem. C **115**, 23081 (2011).
[24] D. J. Singh and L. Nordstrom, *Planewaves, Pseudopotentials, and the LAPW method*, 2nd ed. (Springer, Berlin, 2006).
[25] P. Blaha, K. Schwarz, G. Madsen, D. Kvasnicka, and J. Luitz, WIEN2k, An augmented plane wave+local orbitals program for calculating crystal properties (K. Schwarz, Tech. Univ. Wien, Austria, 2001).

[26] J. P. Perdew, K. Burke, and M. Ernzerhof, Phys. Rev. Lett. **77**, 3865 (1996).
[27] P. H. Dederichs, S. Blugel, R. Zeller, and H. Akai, Phys. Rev. Lett. **53**, 2512 (1984).
[28] K. Schwarz and P. Mohn, J. Phys. F: Met. Phys. **14**, L129 (1984).
[29] V. L. Moruzzi, P. M. Marcus, K. Schwarz, and P. Mohn, Phys. Rev. B **34**, 1784 (1986).
[30] M. W. Lufaso, P. W. Barnes, and P. M. Woodward, Acta Crystallogr., Sect. B: Struct. Sci. **62**, 397 (2006).
[31] G. X. Zhang, A. M. Reilly, A. Tkatchenko, and M. Scheffler, New J. Phys. **20**, 063020 (2018).
[32] Y. Fu and D. J. Singh, Phys. Rev. B **100**, 045126 (2019).
[33] M. Shimizu, Rep. Prog. Phys. **44**, 329 (1981).
[34] A. Aguayo, I. I. Mazin, and D. J. Singh, Phys. Rev. Lett. **92**, 147201 (2004).
[35] P. Larson, I. I. Mazin, and D. J. Singh, Phys. Rev. B **69**, 064429 (2004).
[36] G. Qin, W. Ren, and D. J. Singh, Phys. Rev. B **101**, 014427 (2020).